

Journal of Materials Chemistry A

Accepted Manuscript



This is an *Accepted Manuscript*, which has been through the Royal Society of Chemistry peer review process and has been accepted for publication.

Accepted Manuscripts are published online shortly after acceptance, before technical editing, formatting and proof reading. Using this free service, authors can make their results available to the community, in citable form, before we publish the edited article. We will replace this *Accepted Manuscript* with the edited and formatted *Advance Article* as soon as it is available.

You can find more information about *Accepted Manuscripts* in the [Information for Authors](#).

Please note that technical editing may introduce minor changes to the text and/or graphics, which may alter content. The journal's standard [Terms & Conditions](#) and the [Ethical guidelines](#) still apply. In no event shall the Royal Society of Chemistry be held responsible for any errors or omissions in this *Accepted Manuscript* or any consequences arising from the use of any information it contains.

Capacitive behaviour of functionalized carbon nanotube/ZnO composites coated on glassy carbon electrode

Jagruti S. Suroshe and Shivram S. Garje*

Department of Chemistry, University of Mumbai, Vidyanagari, Santacruz (East), Mumbai-400 098, India

*Author to whom correspondence should be addressed

Email: ssgarje@chem.mu.ac.in, ssgarje@yahoo.com

Tel: +91-22-2654 33 68

Fax: +91-22-2652 85 47

Abstract

An efficient and simple method has been developed to synthesize functionalized multiwall carbon nanotube (FCNTs)/ZnO composites which are employed as supercapacitor (SCs) materials. The multiwall carbon nanotubes (MWCNTs) have been oxidised in presence of concentrated HNO_3 at 120°C for 2 h to generate oxygenated functional groups on the tube-ends along with side walls of FCNTs to enhance their inherent capacitance. The synthesis of FCNTs/ZnO composites have been carried out by solvothermal decomposition of single source precursor (SSP), $\text{ZnCl}_2(\text{benzscz})_2$ (benzscz = benzaldehyde semicarbazone). FCNT/ZnO composites are well characterized by different techniques viz. X-ray diffraction (XRD), Raman spectroscopy, scanning electron microscopy (SEM), transmission electron microscopy (TEM) etc. FCNT/ZnO/glassy carbon (GC) electrodes are fabricated by deposition of FCNT/ZnO composites on the surface of GC which are further tested for their electrochemical performances by cyclic voltammetry (CV), electrochemical impedance spectroscopy (EIS) and chronopotentiometry. FCNT/ZnO composite electrodes show better reversible charging/discharging ability and higher capacitance values compared to bare FCNTs and ZnO electrodes due to synergistic effect of FCNTs and ZnO. Results show that the composite FZ-1 (FCNT/ZnO (1:1)) displays higher capacitance (157 F/g), maximum energy density (32.15 Wh/kg) and good cycle stability. It retains over 96% of its initial specific capacitance even after 1000 cycles.

Keywords: Functionalized carbon nanotubes / ZnO / Solvothermal method / Supercapacitor / single source precursor

1. Introduction

In 21st century, due to environmental issues and depleting fossil fuels there has been increasing demand in developing and refining more efficient energy devices [1, 2]. Among

various power source devices, supercapacitors (SCs) have attracted a great deal of interest over the last decade due to their characteristics such as long cycle life, high power density, fast charge/discharge rates relative to batteries, etc. [3, 4]. According to charge storage mechanism SCs can be classified into two types. First, electrical double layer capacitors (EDLCs), mainly exhibited by carbon materials in which energy can be stored by means of ion adsorption at the electrode/electrolyte interface. Second, pseudocapacitors, demonstrated by metal oxides and conductive polymers which store energy by fast and reversible faradic redox reactions within the electroactive material on the electrode [5, 6].

Electrode materials with high energy, high rate capability and good safety performance are the core part of the SCs to meet the challenging requirements regarding performance of SCs [7]. Carbon materials (carbon nanotubes, carbon spheres, graphene, activated carbon, carbon aerogel etc.), transition metal oxides (MnO_2 , RuO_2 , ZnO , TiO_2 , SnO_2 etc.) and conducting polymers (polyaniline, polypyrrol, polythiophene etc.) have been considered as most promising electrode materials for SCs [1, 8]. Carbon materials provide a fast electron transfer during faradaic charge transfer reactions and hence enhance the capacitance. Additionally, these carbon nanomaterials provide the platform for the decoration of metal oxide nanoparticles (NPs) to avoid their agglomeration which leads to enhanced properties of the NPs [9]. Among the carbon-based materials, carbon nanotubes (CNTs) have been often used as a template for the hybrid assembly of NPs due to their unique properties such as mesoporous character, high surface area, chemical stability, lightweight, low resistivity and compatibility with other materials [10-12].

An enhancement of the compatibility to the composite material can be achieved by a chemical modification of the multiwall carbon nanotubes (MWCNT). Despite the availability of wide range of functionalization methods, oxidation of CNTs using strong oxidising agents is most common and facile approach for the end and side wall functionalization of CNTs [13,

14]. Oxidative methods result into formation of alcohol (C-OH), ketone (C=O), carboxylic (O=C-OH) functional groups which improves the aqueous dispersibility, chemical reactivity and purity of CNTs by removing the metal particles or amorphous carbon from the raw material [15, 16].

ZnO has been considered to be one of the well-known battery active materials having high energy density of 650 Ag^{-1} [17, 18]. ZnO is wide band gap (3.37 eV) n-type semiconductor material which has been widely used in optoelectronic devices such as solar cells, gas sensors, and short-wavelength light - emitting diodes due to their unique electrical, optical and luminescent properties [18-21]. Due to good electrochemical activity and eco-friendly nature, ZnO can be a promising electrode material in SCs [22].

Recently various methods such as magnetic sputtering [23], solvothermal [24], sol process [25], etc. have been reported in the literature to synthesize carbon material/ZnO composites. Aravinda et al. [17] used magnetron sputtering technique for coating ZnO NPs on functionalised multiwall carbon nanotubes (FCNTs). An efficient approach utilizing modified Hummers method, pulse microwave heating, and homogenizing dispersion has been demonstrated by Hsieh et al. [26] to prepare ZnO/graphene hybrid as electrode material for electrochemical capacitors (ECs). D. Kalpana et al. [27] presented new material for symmetric electrochemical supercapacitor in which ZnO with carbon aerogel was used as active material.

The single source precursors (SSPs) have several advantages over multiple source precursors such as precise control over size, shape, particle distribution and it also avoids use of expensive chemicals. SSP contains both metallic as well as non metallic part required for the synthesis of semiconductor NPs. Additionally, the use of SSP minimizes the toxicity and avoids the contamination that occurs on separate introduction of two or more precursors.

In the present study, we have carried out oxidation of MWCNTs using concentrated HNO_3 and characterized by various techniques. We have synthesized FCNT/ZnO composites by successive coating of ZnO NPs on the surface of FCNTs by solvothermal decomposition of SSP i.e. ZnCl_2 (benzscz)₂ (benzscz = benzaldehyde semicarbazone). FCNT/ZnO composites were deposited on the surface of glassy carbon (GC) to fabricate FCNT/ZnO/GC electrodes for SCs. By using cyclic voltammetry (CV), electrochemical impedance spectroscopy (EIS) and chronopotentiometry, we have found that capacitance of FCNTs can be increased after coating of ZnO NPs over FCNTs. To best of our knowledge this is for the first time the use of SSP has been reported for the preparation of FCNT/ZnO composite as a potential electrode material for SCs.

2. Experimental

2.1 Chemicals and solutions

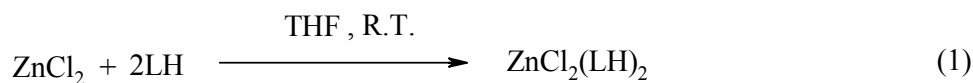
MWCNTs were purchased from Sigma Aldrich. All other chemicals used were of analytical reagent grade. 1M KCl solution was prepared using double distilled water which was employed as an electrolyte in electrochemical capacitor investigation.

2.2 Functionalization of MWCNTs

MWCNTs were refluxed with concentrated HNO_3 at 120°C for 2 h to remove the metal catalyst impurities and generate oxygenated functional groups. The functionalized MWCNTs were thoroughly washed several times with double distilled water until the pH of the filtrate was neutral and dried in an oven at 110°C .

2.3 Synthesis of ZnO NPs and FCNT/ZnO composite.

The SSP, $\text{ZnCl}_2(\text{benzscz})_2$ (benzscz = benzaldehyde semicarbazone) used in the present investigation was prepared by method reported by our group [28]. In this, benzaldehyde semicarbazone dissolved in THF was added to the stoichiometric quantity of ZnCl_2 in THF and the reaction mixture was stirred at room temperature for about 36 h. Then the solvent was removed under vacuum and the resulting white solid was repeatedly washed with cyclohexane to remove any impurities present. The product was dried under vacuum (m. p. 163°C). The reaction scheme (equation 1) is shown below [28].



LH = benzaldehyde semicarbazone

For synthesizing ZnO NPs, in a 250 cm^3 two necked round bottom flask, 20 cm^3 of ethylene glycol was taken and allowed to stir and reflux. In another 100 cm^3 single neck round bottom flask, 100 mg of $\text{ZnCl}_2(\text{benzscz})_2$ was taken in ethylene glycol : distilled water (4:1 ratio) mixture [29]. This solution was then injected with the help of a syringe into a round bottom flask containing refluxing ethylene glycol and refluxed for 2 h. The reaction mixture was allowed to cool to room temperature. The precipitate obtained was centrifuged at 9500 rpm, washed thrice with dry methanol and finally air dried. White colored solid powder obtained was characterized further with UV-Visible spectroscopy (UV-Vis), X-ray diffraction (XRD), scanning electron microscopy (SEM), energy dispersive X-ray analysis (EDAX), transmission electron microscopy (TEM) and Selected Area Electron Diffraction (SAED) techniques.

For the preparation of the composites, in a 250 cm^3 two necked round bottom flask, 100 mg of FCNTs were taken. To this 20 cm^3 of ethylene glycol was added and the flask was sonicated for half an hour. Black colored suspension obtained after sonication was refluxed

with continuous stirring. In another, 100 cm³ single necked round bottom flask, 100 mg of ZnCl₂(benzscz)₂ precursor was taken in ethylene glycol : distilled water (4:1 ratio) mixture. This solution was then injected with the help of syringe into the above refluxing solution of FCNTs in ethylene glycol. The reaction mixture was allowed to reflux for 2 h. It was then cooled to room temperature and the suspension obtained was centrifuged at 9500 rpm, washed thrice with dry methanol and finally dried in air. Black colored solid powder obtained was characterized using UV-Vis, XRD, SEM, EDAX, TEM, SAED, Thermogravimetric analysis (TGA) and Raman spectroscopy.

In this study, three different weight ratios of composite FCNT/ZnO i.e. 1:1, 1:2 and 1:3 were prepared by increasing the amount of precursor i.e. ZnCl₂(benzscz)₂ used for synthesis of ZnO NPs. These composites were represented as FZ-1, FZ-2 and FZ-3 respectively.

2.4 Electrode preparation and electrochemical measurements

The GC electrode surface was polished with 0.5 mm alumina slurries and rinsed thoroughly several times with double distilled water and dried under IR lamp. 4 mg of each sample (FCNTs, ZnO, FZ-1, FZ-2 and FZ-3) were separately dispersed in 2000 μL of ethanol and 6 μL of 5 wt % Naffion by ultrasonication for 60 min to ensure uniformity. 10 μL of these solutions was put on the polished surface of GC to form working electrode and dried under IR lamp to evaporate the solvent. The typical loading amount of the electroactive material on GCE was approximately 0.02 mg cm⁻².

All electrochemical measurements were carried out in a three-electrode configuration. Three electrode assembly consists of a GC electrode (diameter = 3 mm) as a working electrode, platinum wire as counter electrode and Ag/AgCl (Sat. KCl) as a reference electrode. All

voltammetric, chrono and EIS measurements have been performed on Eco Chemie, Electrochemical work station, model Autolab PGSTAT 30 using GPES software, version 4.9.005 and Frequency Response Analyzer (FRA), software version 2.0 respectively.

2.5 Material characterization

The powder XRD studies of the materials were carried on XRD-7000, Shimadzu X-ray diffractometer using CuK_α radiation at a scan rate of 2° min^{-1} . Raman spectra of FCNT and FZ-1, FZ-2 and FZ-3 composites were recorded using 514 nm line from a diode pumped Nd^{3+} : YAG laser (RENISHAW in Via Raman Microscope, Laser 514 nm, Lens 100x). Fourier transform infrared (FTIR) spectra were recorded with Perkin Elmer FTIR spectrophotometer in $4000\text{-}400 \text{ cm}^{-1}$ range. SEM images were taken on a FEI Quanta – 200 scanning electron microscope at an accelerating voltage of 20 kV. EDAX was performed with a spectroscope attached with SEM. For SEM measurements, samples were coated on carbon tape. TEM and SAED were carried out on a PHILIPS, CM 200 microscope with an operating voltage between 20 to 200 kV. Samples for TEM images were prepared by dispersing the dried powder in methanol and placing several drops of the suspension on holey carbon films supported by copper grids. Absorption spectra were recorded using a UV-2450 PC Shimadzu UV-Vis spectrophotometer at room temperature. For absorbance measurements, a weighed dried powder sample was dispersed in methanol and used for recording spectra. The TGA was carried out using Perkin Elmer instrument, Pyris Diamond TG/DTA model with heating rate of $10^\circ \text{Cmin}^{-1}$ in air.

3. Results and discussion

The FZ-1, FZ-2 and FZ-3 composites are synthesized by solvothermal decomposition of $\text{ZnCl}_2(\text{benzscz})_2$ in presence of FCNTs in ethylene glycol : distilled water. $\text{ZnCl}_2(\text{benzscz})_2$ acts as a SSP to give ZnO NPs. The formation of these composites are feasible due to the functionalization of MWCNTs. MWCNTs are often modified covalently by the addition of

polar functional groups. These functional groups promote chemical reactivity and dispersion ability of MWCNTs in organic solvents as well as in aqueous solvents, due to which MWCNTs can be directly used in composite fabrication [30, 31]. In this study, MWCNTs are oxidized using concentrated HNO_3 at 120°C for 2 h. These functionalized MWCNTs are characterized using Infra-Red spectroscopy (IR), Raman spectroscopy and TGA (Supporting Fig. S₁, S₂ and S₄ respectively).

FTIR spectra of untreated MWCNTs and FCNTs are shown in Fig. S₁ (a) and (b). The peak at 3435 cm^{-1} corresponds to stretching of $-\text{OH}$ group and the signal around 2921 cm^{-1} indicate a stretch oscillation from CH_2-CH_3 group. The band observed at 1633 cm^{-1} is assigned to $-\text{C}=\text{O}$ stretching mode of carboxylic acid group. Increase in intensity of peaks for FCNTs compared to untreated MWCNTs indicates the rupture of side walls of MWCNTs after treatment with HNO_3 [32, 33].

The structural changes after acid treatment of the MWCNTs are investigated using Raman spectroscopy. Fig. S₂ (a) and (b) show Raman spectra of untreated MWCNTs and FCNTs. Both the spectra show two characteristic peaks, one at 1354 cm^{-1} and another at 1590 cm^{-1} . The peak observed at 1354 cm^{-1} corresponds to disorder-induced band (D band). 'D' band indicates the disorder features of the CNTs. Another peak observed at 1590 cm^{-1} corresponds to tangential mode (G band). 'G' band is associated with ordered graphite in CNTs. The I_D/I_G ratio is used to estimate amount of defects present in the walls of CNTs. This ratio is found to be 1.148 for MWCNTs and 1.317 for FCNTs. Higher I_D/I_G ratio of FCNTs compared to MWCNTs suggests functionalization of MWCNTs. Higher is the I_D/I_G ratio, more is the functionalization of CNTs [34, 35]. The overtone of 'D' band ('2D' band) is observed at 2691 cm^{-1} and 'D+G' band is observed around 2937 cm^{-1} . The increase in the intensity of '2D' and 'D+G' band of FCNTs compared to MWCNTs indicates increased disorder in FCNTs.

From Fig. S₂, it is also observed that there is an upfield shift of the 'D' band for FCNTs (1354 cm⁻¹) with respect to MWCNTs (1348 cm⁻¹) which confirms the oxidation of MWCNTs. Similar observations have been noticed by Motchelaho et al. during oxidation of CNTs [36].

The TGA of the functionalized carbon nanotubes and the composites were carried out upto 1000°C in air at the heating rate of 10°Cmin⁻¹ in order to estimate ZnO loading amount in the composites. Fig. 1 (a-d) shows TGA of FCNTs, FZ-1, FZ-2 and FZ-3 respectively. As observed in Fig. 1 (a-d) little weight loss is observed around 100°C which is explained by the removal of water adsorbed on the surface of FCNTs and composites. An obvious weight loss in the temperature range 200-650°C is observed for all the materials which is attributed to removal of oxygen containing groups producing CO, CO₂ and H₂O and decomposition of carbon framework from the FCNTs and composites [37, 38]. About 98% weight loss is observed for FCNTs indicating almost complete removal of the material. For composites, FZ-1, FZ-2 and FZ-3 the weight loss is about 85, 79 and 71% respectively. This indicates that the ZnO loading in composites is approximately 13, 19 and 27 wt % respectively [10, 39].

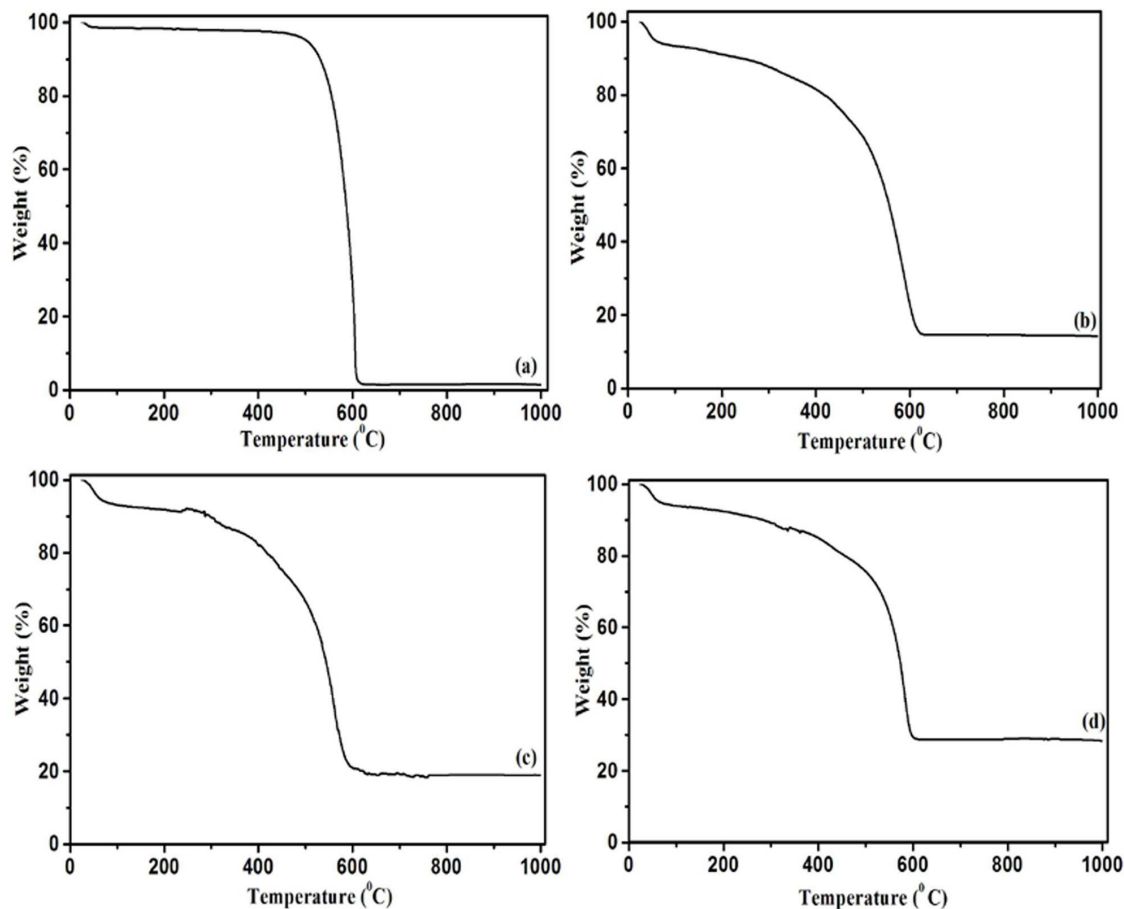


Fig. 1: TGA weight loss curves for (a) FCNT, (b) FZ-1, (c) FZ-2 and (d) FZ-3 with heating rate of $10^{\circ}\text{C min}^{-1}$.

The utility of $\text{ZnCl}_2(\text{benzscz})_2$ as a SSP for obtaining ZnO can be tested from its TGA studies under air. As shown in supporting figure S₃ (a), thermal decomposition of SSP displays a two step degradation mechanism. The first decomposition between 50°C and 100°C is explained by loss of water molecules whereas the gradual weight loss between 120°C to 550°C can be attributed to removal of thermally less stable organic groups followed by loss of inorganic component like chlorides present in the precursor. The weight loss (81.14%) observed in TGA curve under air matches with the one expected (82.41%) for ZnO. Supporting information figure S₃ (b) shows TGA of ZnO NPs. The initial weight loss of ZnO NPs around 100°C to

220^oC is due to evaporation of adsorbed water molecules. The further weight loss observed upto 500 ^oC can be considered to be due to decomposition of organic capping agent surrounding ZnO NPs [40, 41].

TGA profiles of untreated MWCNTs and FCNTs in air are shown in supporting Fig. S₄ (a) and (b). From Fig. S₄ (a) it is observed that TG curve for untreated MWCNTs shows 83% weight loss at 1000^oC. TG curve do not drop to zero weight percent because of presence of metal oxides from metal catalyst used during production of CNTs. These metal oxides are thermally stable and do not decompose even at high temperature. However, TG curve for FCNTs (Fig. S₄ (b)) shows 98% weight loss at 1000^oC which indicates effective removal of metal catalyst after acid treatment. Results obtained from TGA are in good agreement with the results obtained from IR and Raman which ensures oxidation of MWCNTs [42, 43].

The XRD patterns of ZnO NPs, FCNTs, FZ-1, FZ-2 and FZ-3 are shown in Fig. 2 (a)-(e) respectively. The position of diffraction peaks for bare ZnO NPs and ZnO NPs in composites are identical with standard zincite structure (JCPDS File No. 00-036-1451).

The peaks at 2 θ values, 31.7^o, 34.3^o and 36.1^o can be assigned to (100), (002) and (101) crystal planes of hexagonal phase of ZnO, whereas, peaks at 25.8^o and 43.2^o can be ascribed to characteristic (002) and (101) reflections of graphitic plane (JCPDS No. 75-1621). This reveals the crystallinity of FCNTs. XRD patterns of composites, FZ-1, FZ-2 and FZ-3 consists of reflections due to both ZnO NPs as well as FCNTs. No other impurity or additional peaks are seen. Thus, there is exclusive formation of FCNT/ZnO composites.

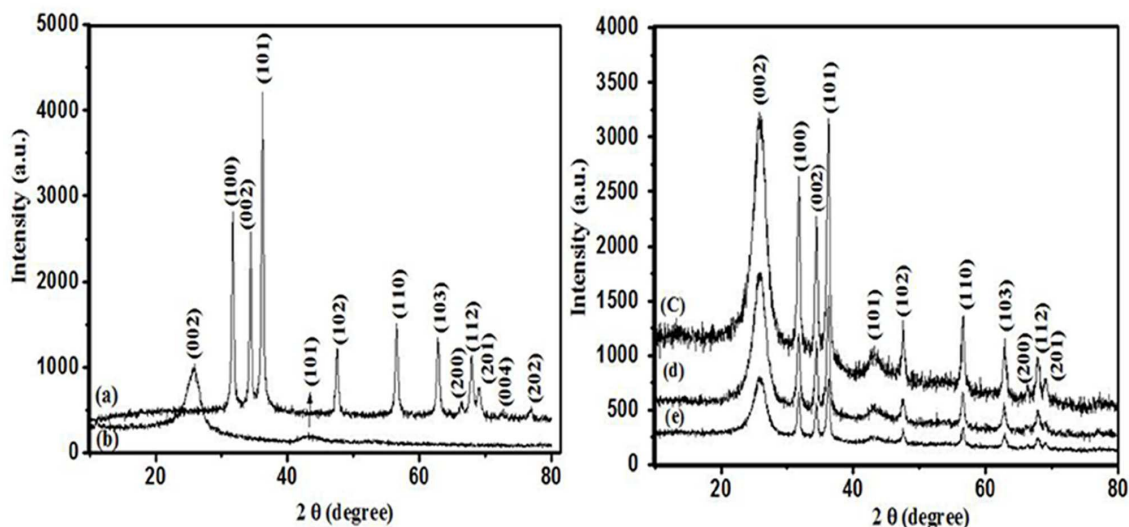


Fig. 2: XRD patterns of (a) Hexagonal ZnO NPs (JCPDS File No. 00-036-1451), (b) FCNTs (JCPDS File No. 75-1621), (c) FZ-1, (d) FZ-2 and (e) FZ-3 composites.

From the XRD, average particle size can be calculated by using the Scherer formula which is shown in equation (2) [27].

$$d = \frac{0.9 \lambda}{\beta \cos \theta} \quad (2)$$

Where, ' λ ' is the wavelength of X-rays (1.5418 \AA), ' θ ' is the Bragg diffraction angle and ' β ' is the full width half maxima.

Based on the XRD data ((101) reflection band), the crystallite size of bare ZnO NPs and ZnO NPs in composites, FZ-1, FZ-2 and FZ-3 are found to be 21.74, 17.97, 7.14 and 7.05 nm respectively.

Fig. 3 (a-h) represents SEM images and EDAX of ZnO NPs, FZ-1, FZ-2 and FZ-3 composites. Fig. 3 (a) shows spherical morphology of the ZnO NPs, whereas, Fig. 3 (b) shows EDAX of the same material. From EDAX, the presence of Zn (45.92%) and O (54.08%) in $\sim 1:1$ stoichiometry can be confirmed. The EDAX spectra of FZ-1, FZ-2 and FZ-3 shows presence of C, Zn and O which confirms the coating of ZnO NPs on the surface of FCNTs.

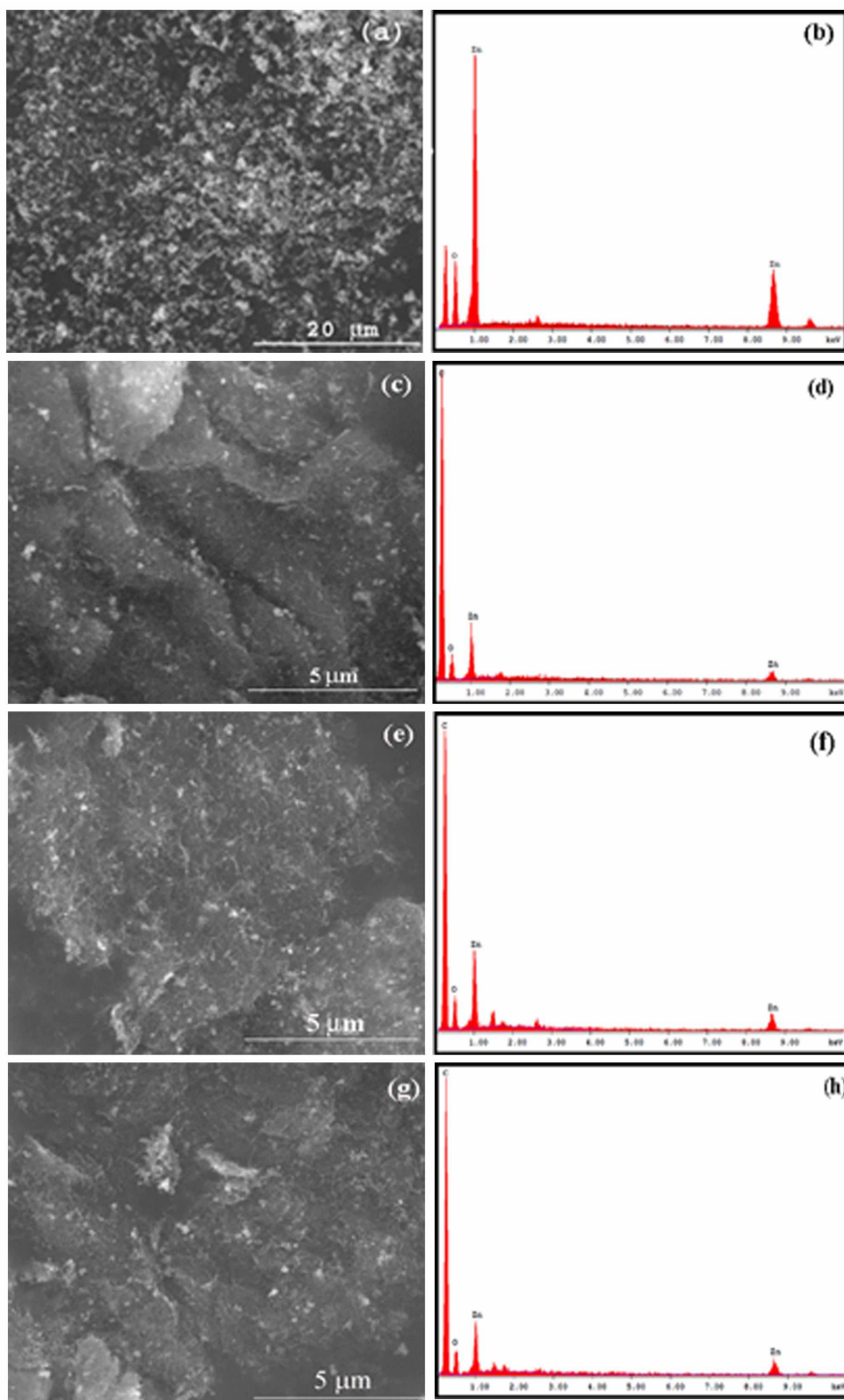


Fig. 3: SEM images and EDAX of ZnO NPs {(a), (b)}, FZ-1 {(c), (d)}, FZ-2 {(e), (f)} and FZ-3 {(g), (h)} composites synthesized using solvothermal method.

Fig. 4 (a-d) shows TEM images of bare ZnO NPs and FZ-1, FZ-2 and FZ-3 composites, respectively. From Fig. 4(a) it can be seen that the bare ZnO NPs have spherical morphology with average particle size around 25 nm. However, some agglomeration is observed. Fig. 4 (b)-(d) clearly shows the coating of ZnO NPs over FCNTs. The average particle sizes of ZnO NPs in FZ-1, FZ-2 and FZ-3 composites are found to be 15, 10 and 12 nm respectively. Fig. S₅ (a-d) represents SAED patterns of bare ZnO NPs, FZ-1, FZ-2 and FZ-3 respectively. Fig. S₅ (b)-(d) clearly indicates (101) graphitic reflection for FCNTs along with reflections for ZnO NPs which confirms formation of FCNT/ZnO composites.

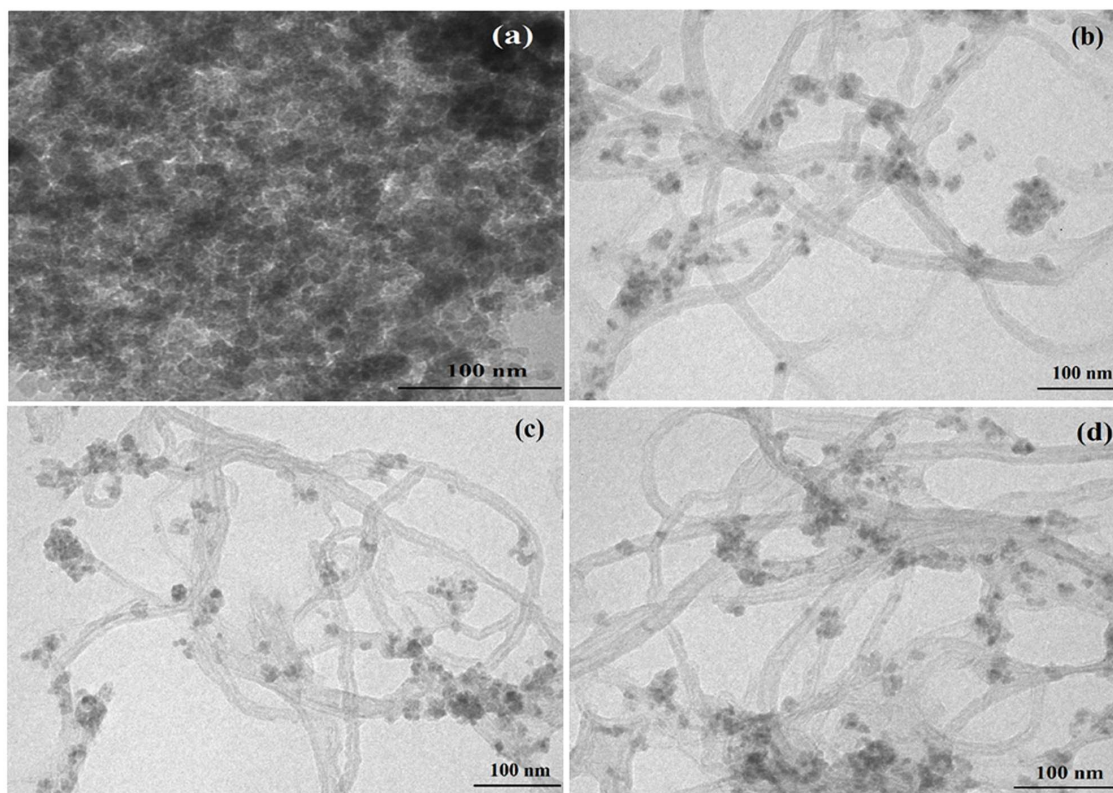


Fig. 4: TEM images of (a) ZnO NPs, (b) FZ-1, (c) FZ-2 and (d) FZ-3 composites.

These composites are also characterized by UV-Vis and Raman spectroscopy (Fig. S₆ and Fig. S₇). Fig. S₆ represents the UV-Visible absorption spectra of FCNTs, ZnO NPs, FZ-1, FZ-2 and FZ-3. FCNTs (Fig. S₆ (b)) exhibited an absorption peak at 254 nm which remains steady in

FZ-1, FZ-2 and FZ-3 composites. This absorption peak corresponds to excitation of π -plasmon of graphitic structure [44]. The ZnO NPs shows absorption at 363 nm (Fig. S₆ (a)) which get blue shifted around 354, 348 and 342 nm in FZ-1, FZ-2 and FZ-3 composites (Fig. S₆ (d), (c) and (e)) respectively. This can be assigned to the quantum size effect of the fine structure in nanometer size [18].

Raman scattering is an essential tool for characterization of carbonaceous materials. The Raman studies provide information about structural disorders and defects in nanostructures.

Raman spectra of FCNTs, FZ-1, FZ-2 and FZ-3 (Fig. S₇) shows two significant bands having peaks at about 1582 and 1354 cm^{-1} . The 'G' band at 1582 cm^{-1} is associated with the E_{2g} phonon mode of sp^2 -hybridized carbon atoms. A distinct band at 1354 cm^{-1} (D band) is associated with the breathing mode of k-point phonons of A_{1g} symmetry [34, 44]. The intensity of the 'D' and 'G' bands (I_D/I_G) of the composites are much lower than that of FCNTs which was attributed to interactions between ZnO NPs and FCNTs. The overtone of 'D' band ('2D' band) observed at 2691 cm^{-1} and 'D+G' band is observed around 2937 cm^{-1} . Decrease in the intensity of '2D' and 'D+G' bands in the all three composites compared to bare FCNTs indicates decreased disorder in the composites after coating of ZnO NPs [45]. All above results indicates successful deposition of ZnO on CNT surface.

The capacitive performances of the FCNTs, ZnO NPs, FZ-1, FZ-2 and FZ-3 composites are evaluated by CV, GCD and EIS techniques in 1 M KCl as an electrolyte. CV measurements of FCNT, ZnO NPs and FCNT/ZnO composites are performed at a constant scan rate of 10 mV/s in the potential window between -0.4 and +0.6 V using three electrode system. Three electrode system has been widely used in electrochemical research and it is considered as a most suitable method [46]. By introducing a reference electrode in three electrode system one can monitor the current between the working and the counter electrode and the voltage between the reference and the working electrode. This is helpful because the potential at the

counter electrode will constantly shift to generate the current demanded by the working electrode [47]. The high values of specific capacitance are observed in three-electrode configuration compared with the two-electrode configuration. This is because in three electrode system, only one electrode, i.e. working electrode contains the material being analysed. Therefore, the applied voltage and current transfer across the single electrode are quite different than in the two electrode system. In a symmetrical two electrode cell the potential difference applied to each electrode are equal to each other and are half the values shown on the X-axis of the cyclic voltammetry. As a result of this for a given potential range on the X-axis in a cyclic voltamogram, the working electrode of a three electrode cell has twice the potential range applied as compared to electrode in two electrode system. This gives rise to approximately double the values of specific capacitance in three electrode cell compared to two electrode cell. This is also evident from the equivalent circuit diagrams of these setups [48-51]. As shown in Fig. 5 (b), the CV of FCNT electrode shows evident redox peaks due to presence of surface oxidation groups i.e. (-COOH, -OH, C=O, -CHO etc.) [10]. It is believed that introduction of oxygen containing functional groups will introduce some negatively charged sites on surface of CNTs which can absorb zinc cations and promote in situ heterogeneous nucleation and growth of ZnO NPs. Such functional groups improve hydrophilicity of CNTs leading to enhanced wettability and also facilitate rapid electrolyte ion transfer within the microspores of the CNTs. Pseudocapacitance induced from the surface oxygenated functional groups also contributes to total capacitance and improve performance of SCs [6, 52].

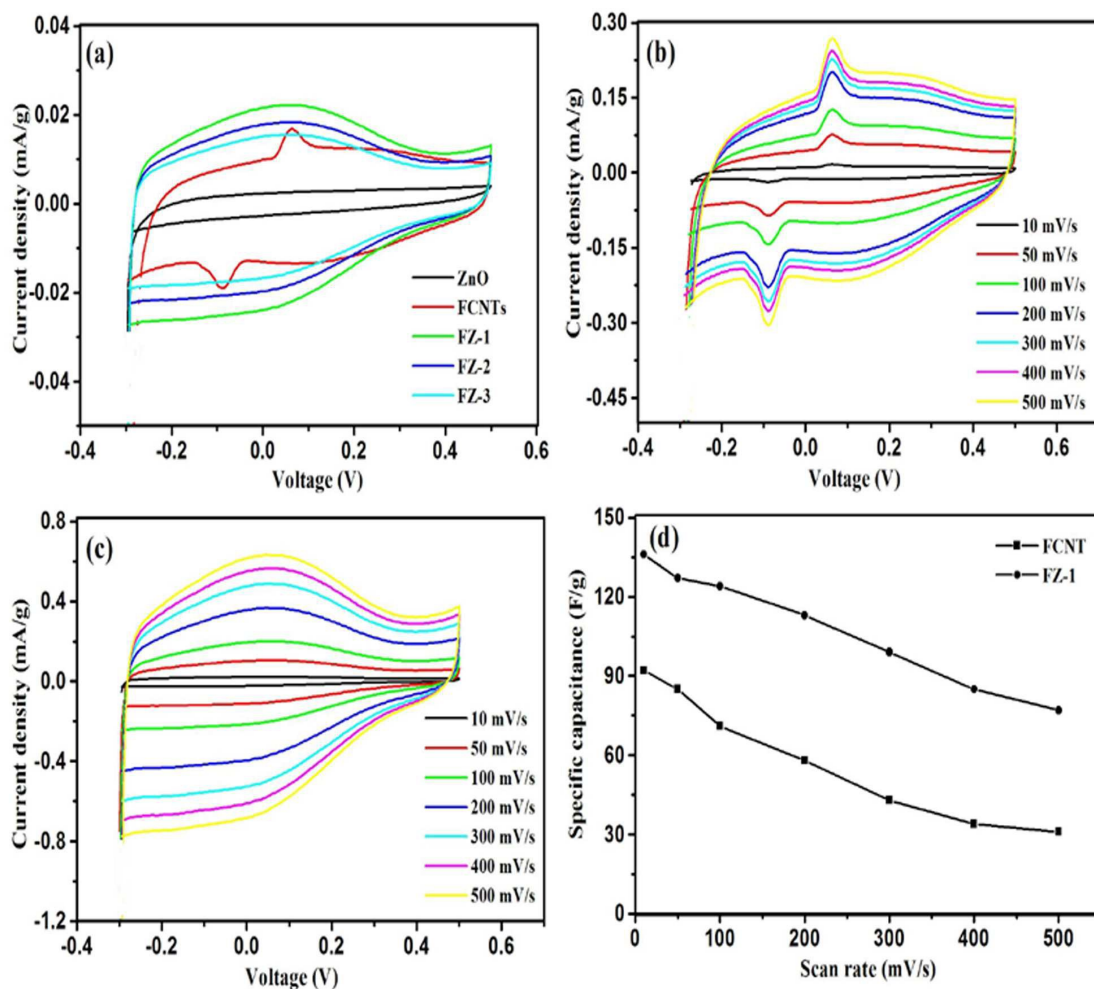


Fig. 5: (a) CV curves of ZnO NPs, FCNT, FZ-1, FZ-2 and FZ-3 at a scan rate of 10 mV/s ; (b) CV curves of FCNT at different scan rates in the range of 10-500 mV/s ; (c) CV curves of FZ-1 at different scan rates in 1M KCl and (d) Specific capacitance vs. scan rate ranging from 10 to 500 mV/s of FCNT and FZ-1 electrodes.

The CV curves of all the materials exhibits rectangular shape, indicating all samples have a good capacitive behaviour. Rectangular type of voltammogram and symmetry in anodic and cathodic directions are characteristics of the good capacitive material [53]. As shown in Fig. 5(a), the CV loops are almost symmetrical in nature. FCNTs and ZnO electrode exhibits specific capacitance of 92 F/g and 30 F/g respectively at scan rate of 10 mV/s. When the

FCNTs are coated with ZnO NPs there is an increase in the capacitance value of the capacitor (FZ-1) up to 136 F/g at scan rate of 10 mV/s. This large enhancement in the capacitance of FCNT/ZnO composites compared to bare FCNT and ZnO is attributed to combined effect of pseudocapacitance of ZnO and double layer capacitance of FCNTs. Presence of conducting ZnO NPs reduces the electrical resistance of the CNTs and increases the charge storage capacity of the composites [54, 55]. The CV curves of the composite electrodes reveal that the mechanism of electrochemical storage can be described by the electrical double layer theory. Energy storage in these electrodes is the accumulation of ionic charge in the double layer at the electrode/electrolyte interface. This may be due to high surface area and the porosity of the FCNTs. Further increase in the coating of ZnO NPs, there is decrease in the capacitance of FZ-2 to 112 F/g and FZ-3 to 99 F/g, still higher than that of bare FCNTs and ZnO NPs. This is because large amount of ZnO NPs covering FCNTs blocks the pores of FCNT electrode and destroys the network structure of the CNT matrix and therefore lowers the conductivity of the electrode. [17, 20].

The CV profile of FCNT and FZ-1 at different scan rate from 10 to 500 mV/s within the potential window of -0.4 to +0.6 V are shown in Fig. 5(b) and (c) respectively. The relative increment in current response with the scan rate indicates an ideal capacitive behavior. The CV curves remain in good rectangular shape even at high scan rate of 500 mV/s. The response of specific capacitance of FCNTs and FZ-1 against the scan rate is also shown in Fig. 5 (d). As the scan rate increases from 10-500 mV/s, area under curve increases and the specific capacitance value decreases. This is because at lower scan rates electrolyte ions are completely diffused into the material and hence all the active surface of material can be utilized for charge storage whereas at high scan rates, diffusion limits the movement of electrolyte ions due to the time constraints and only the outer active surface is used for charge storage [3, 56]. At very low scan rates, scan rate independent behavior of specific capacitance

may be expected. However, internal resistance also plays important role in contributing to specific capacitance. The internal resistance in turn depends on conductivity of electrolyte which is sensitive to electrode spacing. The three electrode cell has larger spacing between electrodes which can result into high equivalent series resistance. This can explain the drastic decrease in specific capacitance with increase in scan rate [48, 57].

The specific capacitance (C_{sp}) is calculated from the CV curves according to equation (3) [58-60].

$$C_{sp} = \frac{i}{s \times m} \quad (3)$$

Where, 'i' is average cathodic current (A), 's' is potential scan rate (V/s) and 'm' is weight of active electrode material (g).

The galvanostatic charge/discharge (GCD) measurements are carried out at various applied currents in order to investigate the capacitive behavior. Fig. 6 (a) displays the galvanostatic charge/discharge curves of ZnO, FCNTs, FZ-1, FZ-2 and FZ-3 electrodes in 1M KCl at a constant current density 0.1 mA/g. The charge/discharge curve exhibits the symmetrical triangular shape employing an ideal capacitor character. The non-linear shape of the discharge curve is observed due to pseudocapacitance behaviour of metal oxides resulting from the electrochemical adsorption-desorption or redox reaction at the electrode and electrolyte interface which is distinct from the linear triangular shape expected from a double layer capacitor. [45, 61]. The specific capacitance (C_{sp}) is also evaluated by chronopotentiometry according to following equation [62].

$$C_{sp} = \frac{I}{[(\Delta V / \Delta t) \times m]} \quad (4)$$

Where 'I' is constant current density (A/g), ' ΔV ' is discharging potential difference range, ' Δt ' is discharge time and 'm' is weight of active electrode material (g).

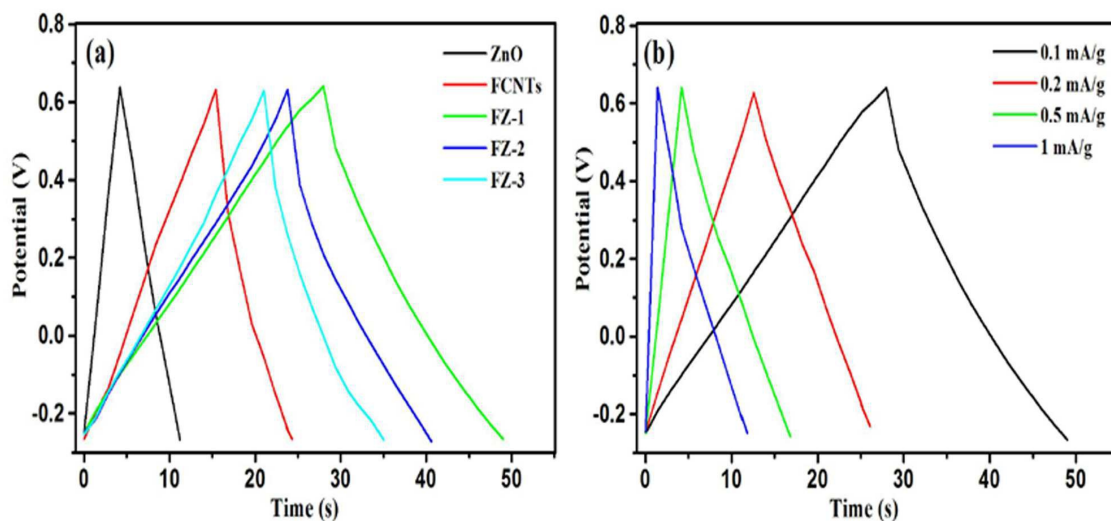


Fig. 6: (a) GCD curves for ZnO NPs, FCNT, FZ-3, FZ-2 and FZ-1 at a constant current density of 0.1 mA/g and (b) GCD curves for FZ-1 at different current densities from 0.1 to 1 mA/g.

The C_{sp} values of the ZnO, FCNTs, FZ-1, FZ-2 and FZ-3 electrodes from Fig. 6 (a) are about 24, 86, 157, 135 and 119 F/g respectively at 0.1 mA/g. The GCD curves for FZ-1 capacitor at different current densities are depicted in Fig. 6 (b). It can be found that the charging curves are symmetric to its corresponding discharging counterpart for both the capacitors. As expected FZ-1 capacitor displays higher specific capacitance than the FCNTs, FZ-2 and FZ-3. The excellent electrochemical performances of FCNT/ZnO composites compared to bare FCNTs and ZnO NPs are attributed to unique microstructure of composites. ZnO NPs coated over the surface of FCNTs accumulate to form the pores for ion-buffering reservoirs to improve diffusion rate of ions. The large specific surface area and nano size ZnO particles of the FCNT/ZnO composites greatly reduce the diffusion length over which both ions and electrons must transfer during charge/discharge process. The excellent interfacial contact between ZnO and FCNTs facilitates fast electron and ion transport simultaneously throughout the whole electrode matrix and hence presenting the best electrochemical capacitive

performance [1, 44]. Furthermore, the IR drop at the initial discharge is observed due to higher internal resistance of the electrolyte [63, 64].

The energy density (E) and power density (P) are calculated from galvanostatic charge/discharge curves using equations (5) and (6) [65].

$$E = \frac{1}{2} C_{sp} V_i^2 \quad (5)$$

$$P = \frac{E}{T_d} \quad (6)$$

Where, ' C_{sp} ' is specific capacitance (F/g), ' V_i ' is maximum voltage (V) and ' T_d ' is discharge time (s).

Fig. 7. shows the Ragone plot which shows relationship between energy density and power density. It can be seen that with increase in current density there is decrease in energy density and increase in power density. The decreasing fashion of specific energy suggests that parts of the surface of the electrodes are inaccessible at high charge-discharging current [49, 53]. The absence of plateau region in the Ragone plot shows that the ratio between energy and power known as time of discharge (or charge) decreases rapidly. Such capacitors can be used in low current application devices. Increasing trend in power density suggest that discharging capacity of supercapacitor is directly proportional to current density. The FZ-1 shows best performance with energy density of 32.15 Wh/kg and power density of 1.15 kW/kg respectively at a current density 0.1 mA/g.

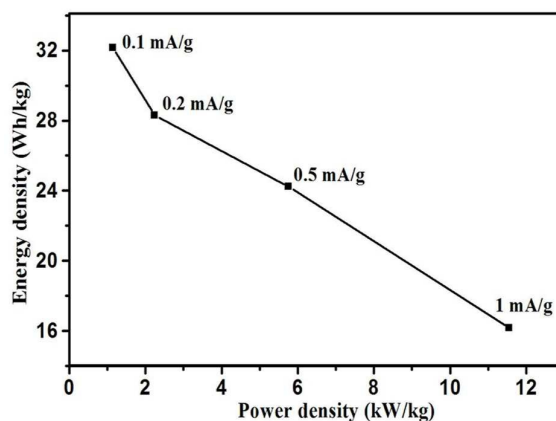


Fig. 7: Ragone plot for FZ-1 electrode at different current densities from 0.1 mA/g to 1 mA/g.

The cycle stability of SCs is also an important parameter for their practical applications. In order to evaluate stability of FCNT and FCNT/ZnO composites the cycling test is performed for the 1000 cycles at scan rate of 100 mV/s. Fig. 8 (a) represents cyclic stability of FZ-1 composite. There is negligible decrease in specific capacitance even after 1000 cycles. This may be due to increased internal resistance during cycling. As shown in Fig. 8 (b), at 100 mV/s the specific capacitance of FZ-1 is 124 F/g at first cycle and decreases to 118 F/g after 1000 cycles, with retention of 96% specific capacitance. Whereas the specific capacitance of FZ-2 and FZ-3 in the first cycle are 95 F/g (93% retention after 1000 cycles), 81 F/g (91% retention after 1000 cycles) respectively. From Fig. 8 (b), it is also observed that for FZ-3 composite at 600 cycles there is increase in specific capacitance which is because of increase in temperature of electrolyte after continuous operation for several hours [62]. Supporting figure S₈ represents coulombic efficiency of the composites at a constant current density of 0.1 mA/g. The coulombic efficiency (η) is calculated from its charging (T_c) and discharging (T_d) times using following equation [66].

$$\eta = \frac{T_d}{T_c} \times 100 \quad (7)$$

Where, 'T_d' and 'T_c' are discharging and charging times. The initial coulombic efficiency of the FZ-1, FZ-2 and FZ-3 composites are found to be 88, 85 and 83% which is further reduced to 86, 82 and 80% after 1000 cycles. These results show good cycle stability which is consistent with the cycle stability tested by CV.

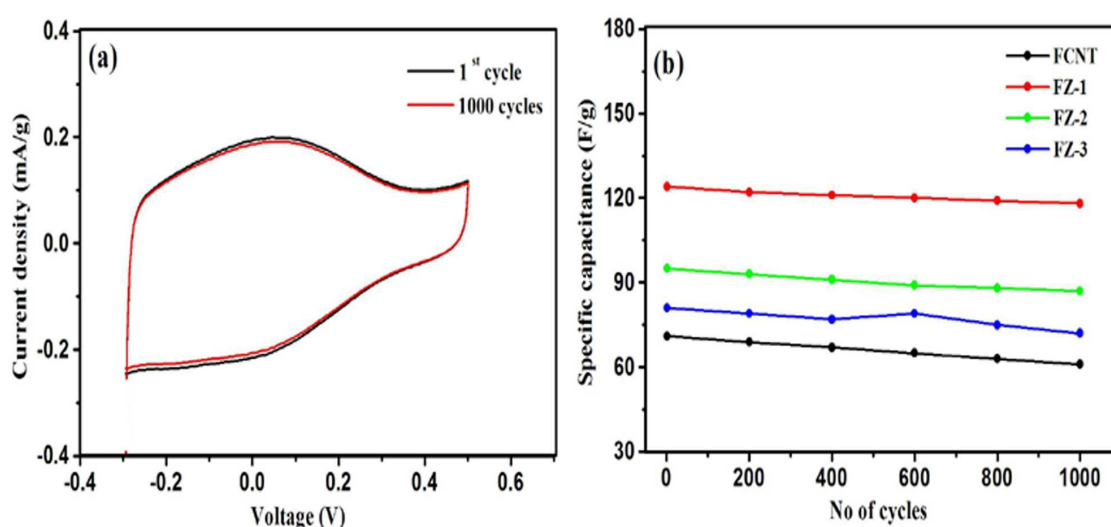


Fig. 8: (a) Cyclic performance of FZ-1 electrode at a scan rate 100 mV/s for 1st cycle and after 1000 cycles and (b) Variation of specific capacitance with increasing no. of cycles for FZ-1, FZ-2, FZ-3 and FCNT at 100 mV/s based on CV data.

Overall results shows that among all composites FZ-1 composite electrode has large specific capacitance with good cycling stability, which is promising for the development of SCs. The excellent performance of composite electrode can be attributed to large surface area and high chemical stability of FCNTs. The combination of ZnO NPs and FCNTs can be utilized as an active electrode material for SCs [44, 67].

The EIS analysis is used to study the fundamental behaviour of electrode materials for SCs. For further understanding, impedance of FCNTs, ZnO NPs, FZ-1, FZ-2 and FZ-3 composites are measured in the frequency range of 0.1 Hz to 10^6 Hz. The EIS data is analyzed using Nyquist plots, which shows the frequency response of the electrode/electrolyte system plotted with the imaginary component ($-Z''$) of the impedance against the real component (Z'). Fig. 9 shows the Nyquist plots for FCNTs, ZnO NPs, FZ-1, FZ-2 and FZ-3 composite electrodes. Each impedance spectrum has a semicircle arc in the high frequency range and straight line in the low frequency range. The high frequency arc represents the charge transfer limiting process occurring at the electrode/electrolyte interface which corresponds to charge transfer resistance (R_{ct}) caused by faradic reactions and double layer capacitance (C_{dl}) on the grain surface [68].

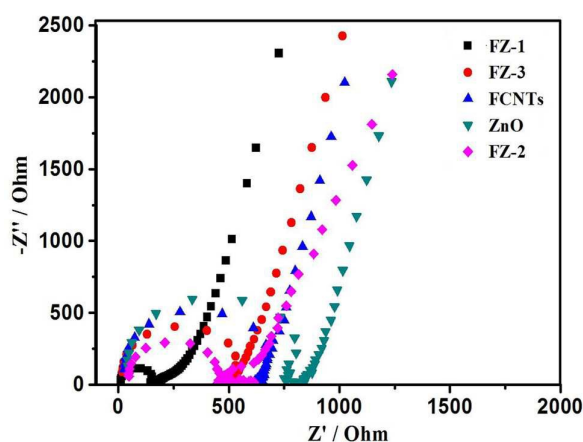


Fig. 9: Nyquist plots of FCNTs, ZnO NPs, FZ-1, FZ-2 and FZ-3 composites.

At low frequencies, the impedance plot should be a vertical line which is parallel to the imaginary axis. The low frequency segment with slope gradually changing from 45^0 to 90^0 represents the diffusion of ions in the electrode material [68]. However, the low frequency straight line departs from those expected with a slope angle smaller than $\pi/2$ for these

electrodes can be explained by the electrode surface inhomogeneity and the existence of “constant phase element” [69, 70].

It is seen from Nyquist plot that the diameter of semicircle goes on decreasing from ZnO NPs to FZ-1 composite. R_{ct} values are directly measured as the semicircle arc diameter. The values of R_{ct} from the semicircle loop of the Nyquist plot are found to be 0.85, 0.76, 0.31, 0.57 and 0.67 K ohms for ZnO NPs, FCNTs, FZ-1, FZ-2 and FZ-3 respectively. The Nyquist plot in low frequency region is vertical line for an ideal material. The Nyquist plot for FZ-1 composite shows vertical line almost parallel to imaginary axis compared to ZnO NPs, FCNTs, FZ-2 and FZ-3 which suggests good capacitive behaviour of composite electrode. Composites shows better charge transfer compared to ZnO NPs and FCNTs. This is because presence of ZnO NPs on FCNTs offers resistance to the diffusion of the electrolyte ions within the pores of the FCNTs which improves the charge transfer performance of FCNT/ZnO electrodes. The R_{ct} values increases as the coating of ZnO NPs on FCNTs increases. This is due to increase in electronic resistance which is attributed to broad band gap and poor conductivity of ZnO NPs.

FZ-1 composite exhibits the smallest R_{ct} of 0.31 K Ω , indicating the optimal composition of CNTs and ZnO that lowers the inter-granular electronic resistance among active materials and the contact resistance between the electrode and the current collector [20, 56].

4. Conclusion

FCNT/ZnO composites as electrodes for supercapacitors were fabricated by solvothermal decomposition of single source precursor. The surface morphology, structure and capacitive behaviors of FCNTs, ZnO and FCNTs/ZnO composites were investigated. The incorporation of ZnO on the surface of FCNTs improves the capacitance of composite electrode, the electrolyte/electrode accessibility as well as conductivity. Controlling the ratio of ZnO to FCNTs is very important to obtain good electrochemical performance. All the composite

electrode materials show high capacitance value, good reversible charge/discharge ability compared to bare FCNTs and ZnO electrodes. Among composite electrodes, FZ-1 exhibits highest specific capacitance of 157 F/g at constant current density of 0.1 mA/g in 1M KCl and energy density of 32.15 kW/kg. Even after 1000 cycles, FZ-1 composite electrode maintains 96% of its initial specific capacitance which serves them as a promising electrode material for supercapacitors.

Acknowledgement

The Authors wish to acknowledge Icon analytical laboratory and SAIF, IIT Bombay for providing SEM and TEM facility. Thanks are also due to Prof. A. K. Srivastava for providing electrochemical workstation facility.

References

- [1] W. Yang, Z. Gao, J. Wang, B. Wang, Q. Liu, Z. Li, T. Mann, P. Yang, M. Zhang and L. Liu, *Electrochim. Acta.*, 2012, **69**, 112-119.
- [2] F. Cao, G. X. Pan, X. H. Xia, P. S. Tang and H. F. Chen, *J. Power Sources*, 2014, **264**, 161-167.
- [3] J. H. Chen, W. Z. Li, D. Z. Wang, S. X. Yang, J. G. Wen and Z. F. Ren, *Carbon*, 2002, **40**, 1193-1197.
- [4] J. Chen, N. Xia, T. Zhou, S. Tan, F. Jiang and D. Yuan, *Int. J. Electrochem. Sci.*, 2009, **4**, 1063-1073.
- [5] M. Selvakumar and D. K. Bhat, *Appl. Surf. Sci.*, 2012, **263**, 236-241.
- [6] Y. Jang, J. Jo, Y. M. Choi, I. Kim, S. H. Lee, D. Kim and S. M. Yoon, *Electrochim. Acta.*, 2013, **102**, 240-245.
- [7] J. Ren, J. Yang, A. Abouimrane, D. Wang and K. Amine, *J. Power Sources*, 2011, **196**

- 8701–8705.
- [8] Y. Zhang, H. Li, L. Pan, T. Lu and Z. Sun, *J. Electroanal. Chem.*, 2009, **634**, 68–71.
- [9] A. K. Mishra and S. Ramaprabhu, *J. Phys. Chem. C*, 2011, **115**, 14006–14013.
- [10] C. T. Hsieh, Y. C. Chen, Y. F. Chen, M. M. Huq, P. Y. Chen and B. S. Jang, *J. Power Sources*, 2014, **269**, 526–533.
- [11] Y. Zhu, H. I. Elim, Y. L. Foo, T. Yu, Y. Liu, W. Ji, J. Y. Lee, Z. Shen, A. T. S. Wee, J. T. L. Thong and C. H. Sow, *Adv. Mater.*, 2006, **18**, 587–592.
- [12] G. Arabale, D. Wagh, M. Kulkarni, I. S. Mulla, S. P. Vernekar, K. Vijayamohan and A. M. Rao, *Chem. Phys. Lett.*, 2003, **376**, 207–213.
- [13] F. H. Gojny, J. Nastalczyk, Z. Roslaniec and K. Schulte, *Chem. Phys. Lett.*, 2003, **370**, 820–824.
- [14] S. Kumar, M. Das, R. P. Singh, S. Datir, D. S. Chauhan and S. Jain, *Colloids Surf. A Physicochem. Eng. Asp.*, 2013, **419**, 156–165.
- [15] A. M. D. Silva, H. F. D. Santos and P. Giannozzi, *Chem. Phys. Lett.* 2013, **582**, 123–128.
- [16] N. G. Sahoo, S. Rana, J. W. Cho, L. Li and S. H. Chan, *Prog. Polym. Sci.*, 2010, **35**, 837–867.
- [17] L. S. Aravinda, K. K. Nagaraja, H. S. Nagaraja, K. U. Bhat and B. R. Bhat, *Electrochim. Acta.*, 2013, **95**, 119–124.
- [18] A. Ramadoss and S. J. Kim, *Mater. Chem. Phys.*, 2013, **140**, 405–411.
- [19] Y. Z. Liu, Y. F. Li, Y. G. Yang, Y. F. Wen and M. Z. Wang, *Scripta Mater.*, 2013, **68**, 301–304.
- [20] Y. Zhang, X. Sun, L. Pan, H. Li, Z. Sun, C. Sun and B. K. Tay, *Solid State Ionics*, 2009, **180**, 1525–1528.
- [21] D. S. Kim, S. M. Lee, R. Scholz, M. Knez, U. Gosele, J. Fallert, H. Kalt and M.

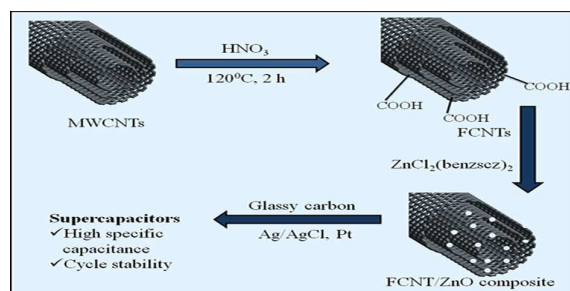
- Zacharias, *Appl. Phys. Lett.*, 2008, **93**, 103-108.
- [22] M. Selvakumar, D. K. Bhat, A. M. Aggarwal, S. P. Iyer and G. Sravani, *Physica B*, 2010, **405**, 2286–2289.
- [23] N. Ouldhamadouche, A. Achour, I. Musa, K. A. Aissa, F. Massuyeau, P. Y. Jouan, M. Kechouane, L. L. Brizoual, E. Faulques, N. Barreau and M. A. Djouadi, *Thin Solid Films*, 2012, **520**, 4816–4819.
- [24] S. Lian, H. Huang, J. Zhang, Z. Kang and Y. Liu, *Solid State Commun.*, 2013, **155**, 53–56.
- [25] L. P. Zhu, G. H. Liao, W. Y. Huang, L. L. Ma, Y. Yang, Y. Yu and S. Y. Fu, *Mater. Sci. Eng. B*, 2009, **163**, 194–198.
- [26] C. T. Hsieh, J. S. Lin, Y. F. Chen, C. Y. Lin and W. Y. Li, *Mater. Chem. Phys.*, 2014, **143**, 853-859.
- [27] D. Kalpana, K. S. Omkumar, S. S. Kumar and N. G. Renganathan, *Electrochim. Acta.*, 2006, **52**, 1309–1315.
- [28] A. M. Palve and S. S. Garje, *Synth. React. Inorg. Met.-Org. Nano-Met. Chem.*, 2010, **40**, 153-156.
- [29] V. S. Marques, L. S. Cavalcante, J. C. Sczancoski, A. F. P. Alcantara, M. O. Orlandi, E. Moraes, E. Longo, J. A. Varela, M. S. Li and M. R. M. C. Santos, *Cryst. Growth Des.*, 2010, **10**, 4752-4768.
- [30] K. A. Wepasnick, B. A. Smith, K. E. Schrote, H. K. Wilson, S. R. Diegelmann and D. H. Fairbrother, *Carbon*, 2011, **49**, 24-26.
- [31] Y. R. Shin, I. Y. Jeon and J. B. Baek, *Carbon*, 2012, **50**, 1465-1476.
- [32] D. Bikiaris, A. Vassiliou, K. Chrissafis, K. M. Paraskevopoulos, A. Jannakoudakis and A. Docoslis, *Polym. Degrad. Stab.*, 2008, **93**, 952-967.
- [33] F. C. Moraes, M. F. Cabral, L. H. Mascaro and S. A. S. Machado, *Surf. Sci.*, 2011, **605**

- 435-440.
- [34] C. Dong, A. S. Campell, R. Eldawud, G. Perhinschi, Y. Rojanasakul and C. Z. Dinu, *Appl. Surf. Sci.*, 2013, **264**, 261–268.
- [35] M. A. Pimenta, G. Dresselhaus, M. S. Dresselhaus, L. G. Cancado, A. Jorio and R. Saito, *Phys. Chem. Chem. Phys.*, 2007, **9**, 1276–1291.
- [36] M. A. M. Motchelaho, H. Xiong, M. Moyo, L. L. Jewell and N. J. Coville, *J. Mol. Catal. A: Chem.* 2011, **335**, 189–198.
- [37] A. R. Marlinda, N. M. Huang, M. R. Muhamad, M. N. An'amt, B. Y. S. Chang, N. Yusoff, I. Harrison, H. N. Lim, C. H. Chia and S. V. Kumar, *Mater. Lett.* 2012, **80**, 9-12.
- [38] Y. Yang and T. Liu, *Appl. Surf. Sci.*, 2011, **257**, 8950–8954.
- [39] C. T. Hsieh, Y. T. Lin, W. Y. Chen and J. L. Wei, *Powder Technol.*, 2009, **192**, 16-22.
- [40] P. C. Nagajyothi, S. J. Cha, I. J. Yang, T. V. M. Sreekanth, K. J. Kim and H. M. Shin, *J. Photochem. Photobiol. B*, 2015, **146**, 10-17.
- [41] Shamsuzzaman, A. Ali, M. Asif, A. Mashrai and H. Khanam, *Eur. Chem. Bull.*, 2014, **3**, 939-945.
- [42] H. Gong, S. T. Kim, J. D. Lee and S. Yim, *Appl. Surf. Sci.*, 2013, **266**, 219–224.
- [43] B. Boussouari and M. Baitoul, *J. Mater. Sci. Eng. Adv. Technol.*, 2014, **9**, 1-15.
- [44] K. S. Subrahmanyam, S. R. C. Vivekchand, A. Govindaraj and C. N. R. Rao, *J. Mater. Chem.*, 2008, **18**, 1517–1523.
- [45] Y. Haldorai, W. Voit and J. J. Shim, *Electrochim. Acta*, 2014, **120**, 65-72.
- [46] S. Zhang and N. Pan, *Adv. Energy Mater.*, 2014, **5**, 1401401 (1-19).
- [47] J. Prasek, L. Trnkova, I. Gablech, P. Businova, J. Drbohlavova, J. Chomoucka, V. Adam, R. Kizek and J. Hubalek, *Int. J. Electrochem. Sci.*, 2012, **7**, 1785 – 1801.
- [48] M. D. Stoller and R. S. Ruoff, *Energy Environ. Sci.*, 2010, **3**, 1294-1301.
- [49] D. Qu and H. Shi, *J. Power Sources*, 1998, **74**, 99-107.
- [50] V. Khomenko, E. Frackowiak and F. Beguin, *Electrochim. Acta*, 2005, **50**, 2499-2506.

- [51] T. Chen and L. Dai, *J. Mater. Chem. A*, 2014, **2**, 10756-10775.
- [52] G. Wang, L. Zhang, J. Zhang, *Chem. Soc. Rev.*, 2012, **41**, 797–828.
- [53] G. S. Gund, D. P. Dubal, B. H. Patil, S. S. Shinde and C. D. Lokhande, *Electrochim. Acta*, 2013, **92**, 205– 215.
- [54] B. E. Conway, V. Birss and J. Wojtowicz, *J. Power Sources*, 1997, **66**, 1-14.
- [55] R. A. Fisher, M. R. Watt and W. J. Ready, *J. Solid State Sci. Technol.*, 2013, **2**, M3170-M3177.
- [56] Z. Li, Z. Zhou, G. Yun, K. Shi, X. Lv and B. Yang, *Nanoscale Research Lett.*, 2013, **8**, 473- 482.
- [57] D. P. Dubal, G. S. Gund, R. Holze, H. S. Jadhav, C. D. Lokhande and C. J. Park, *Dalton Trans.* 2013, **42**, 6459-6467.
- [58] Q. Yang, Z. Lu, X. Sun and J. Liu, *Sci. Rep.* 2013, **3**, 3537; DOI:10.1038/srep03537.
- [59] J. P. Zheng, P. C. Goonetilleke, C. M. Pettit and D. Roy, *Talanta*, 2010, **81**, 1045-1055.
- [60] J. Mu, B. Chen, Z. Guo, M. Zhang, Z. Zhang, P. Zhang, C. Shao and Y. Liu, *Nanoscale*, 2011, **3**, 5034-5040.
- [61] X. H. Xia, J. P. Tu, X. L. Wang, C. D. Gu, X. B. Zhao, *Chem. Commun.*, 2011, **47**, 5786–5788.
- [62] P. K. Kalambate, R. A. Dar, S. P. Karna and A. K. Srivastava, *J. Power sources*, 2015, **276**, 262-270.
- [63] M. Zhou, T. Tian, X. Li, X. Sun, J. Zhang, Y. Chen, P. Cui, J. Tang and L. C. Qin, *Chem. Phys. Lett.* 2013, **581**, 64-69.
- [64] Y. Liu, Y. Zhang, G. Ma, Z. Wang, K. Liu and H. Liu, *Electrochim. Acta*, 2013, **88**, 519-525.
- [65] S. Li, J. Wen, X. Mo, H. Long, H. Wang, J. Wang and G. Fang, *J. Power Sources*, 2014, **256**, 206-211.

- [66] B. Vidhyadharan, I. I. Misnon, R. A. Aziz, K. P. Padmasree, M. M. Yusoffa and R. Jose, *J. Mater. Chem. A*, 2014, **2**, 6578-6588.
- [67] W. Yang, Z. Gao, J. Ma, J. Wang, B. Wang and L. Liu, *Electrochim. Acta*, 2013, **112**, 378-385.
- [68] Y. Zhao, Y. Meng and P. Jiang, *J. Power Sources*, 2014, **259**, 219-226.
- [69] R. D. Levie, *Electrochim. Acta*, 1964, **9**, 1231-1245.
- [70] T. Pajkossy, *Solid State Ionics*, 2005, **176**, 1997 – 2003.

Graphical abstract



Synthesis, characterization of functionalized carbon nanotube/ZnO composites by solvothermal decomposition of single source precursor and their use as electrode material for supercapacitors with good reversible charge/discharge ability and cycle stability.